ELSEVIER

Materials Science and Engineering A297 (2001) 203–211

MATERIALS SCIENCE & ENGINEERING A

www.elsevier.com/locate/msea

Quasi-static and dynamic mechanical response of *Strombus gigas* (conch) shells

R. Menig [a], M.H. Meyers [b,1], M.A. Meyers [c,*], K.S. Vecchio [c]

[a] *Institute for Materials Science I, University of Karlsruhe (TH), Germany*
[b] *Department of Biology, University of California, San Diego, CA, USA*
[c] *Department of Mechanical and Aerospace Engineering, University of California, 900 Gilman Drive, La Jolla, CA 92093-0411, USA*

Received 3 November 1999; received in revised form 26 May 2000

Abstract

Quasi-static and dynamic compression and three-point bending tests have been carried out on *Strombus gigas* (conch) shells. The mechanical response is correlated with its microstructure and damage mechanisms. The mechanical response is found to vary significantly from specimen to specimen and requires the application of Weibull statistics in order to be quantitatively evaluated. The conch exhibited orientation dependence of strength as well as significant strain-rate sensitivity; the failure strength at loading rates between 10×10^3 and 25×10^3 GPa s^{-1} was approximately 50% higher than the quasi-static strength. Quasi-static compressive failure occurred gradually, in a mode sometimes described as 'graceful failure'. Crack deflection, delocalization of damage, and viscoplastic deformation of the organic layers are the most important mechanisms contributing to the unique mechanical properties of these shells.

Keywords: Shells; Mechanical properties; Conch; Dynamic properties

1. Introduction

In biological structural systems, the separation between materials and structures, present in most of our contemporary designs, does not exist. Structures and materials are fully integrated in natural organisms. The hierarchical organization of the structure at different spatial scales (nano, micro, meso, macro) is inherent to these systems. The modern approach to design, as described by Ashby [1], integrates the selection of materials into the structure. The design of hierarchically organized materials is an important contemporary research area [2,3], and biological structural systems are excellent models [4] for advanced materials, yet to be developed.

Examples of the unique properties of biological structural systems abound (Vincent [4], Srinivasan et al. [5]). For example, there is a crustacean (*Gorodactilis chiragra*) that uses its forelinks as a catapult to break mollusk, in a similar manner to a Karate chop [4]; the hardness of the forelink exceeds 1 GPa. The marine sponge, Monoraphis, has a silica rod with several mm diameter and up to 1 m long which is used to anchor itself to coral or rock [4]. This rod has extraordinary high flexure strength. It can undergo a deflection that is seven times higher than conventional glass, and has a flexure strength four times higher than glass. These unique properties are due to a structure made of concentric rings, which are hierarchically organized, minimizing and localizing damage. Silk is yet another example of a biological material with high strength; the Araneus siricatus (Spider web) tensile strength approaches 1 GPa. This high strength is coupled with a considerable resilience and toughness; the corresponding breaking energy is approximately 160 MJ m^{-3}. These properties have evolved through millions of years of evolution through a natural selection process.

Mollusks are known to possess hierarchical structures highly optimized for toughness. The two mollusks that have been most studied are *Haliotis rufescens* (abalone) and *Pinctata* (conch) shells. If one considers

* Corresponding author. Tel.: +1-858-5344719; fax: +1-858-5345698.
E-mail address: mamyers@mae.ucsd.edu (M.A. Meyers).
[1] Currently at Gen-Probe, San Diego, CA, USA.

0921-5093/01/$ - see front matter
PII: S0921-5093(00)01228-4

the weak constituents from which the shells are made — namely calcium carbonate ($CaCO_3$) and a series of organic binders [6,7], the mechanical properties of these shells are outstanding. Their tensile strength varies between 100 and 300 MPa, and fracture toughness between 3 and 7 MPa m^{-2}. $CaCO_3$ has corresponding strength and toughness values of 30 MPa and < 1 MPa m^{-2}, respectively. These mollusks owe their extraordinary mechanical properties to hierarchically organized structure starting with single crystals of $CaCO_3$, with dimensions of 4–5 nm (nanostructure), and proceeding with 'bricks' with dimensions of 0.5–10 μm (microstructure), and finishing with layers of 0.2 mm (mesostructure). One of the principal attributes of mollusk response to loads is the graceful (or gradual) failure, in contrast with monolithic ceramics, which exhibit a sudden, or catastrophic failure through the propagation of a crack through the entire specimen.

Based on this concept, Sarikaya et al. [8] developed a B_4C–Al laminated composite 70% $B_4C + 30\%$ Al. The same dramatic improvement in properties with respect to monolithic B_4C is observed: a two- to three-fold increase in both properties is obtained.

The objectives of this work are to evaluate the static and dynamic response and evolution of damage in pink conch (*Strombus gigas*). To date the dynamic properties have not been established, and previous mechanical testing has been restricted to three and four-point bending. Little is known about the mechanisms of compressive failure, as well as about the effect of loading rate on their response.

The ultimate goal of this research program is to understand the positive engineering properties exhibited by hierarchical multiphase complex natural composites in order to design and synthesize multi-functional composites tailored to optimize structural plus ballistic and/or blast applications. The design of hierarchically organized materials is an important contemporary research area, and biological structural systems are excellent models for the design of advanced materials yet to be envisioned. The rapid development in understanding the structure and deformation mechanisms in natural systems is enabling materials scientists to begin developing synthetic composite materials which mimic the behavior and performance advantages of their natural counterparts. The synthesis, processing, characterization, and material modeling of laminate, segmented and 3D composites designed to optimally incorporate and simultaneously exploit 'multiple' energy dissipation mechanisms is a possible outcome of this research. Some of these mechanisms are: plasticity in the ductile layers, fragmentation of the hardened layers, accommodation mechanisms through sliding and rotation, crack deflection due to the anisotropic nature of the layers, pullout of individual 'tiles'. The design of these composite materials is based on lessons learned from nature through research into the mechanical properties and damage evolution in shells; these mechanisms operate at the macro(structural)-, meso- and micro-levels and optimize the impact resistance, an important characteristic in enhancing ballistic and blast performance.

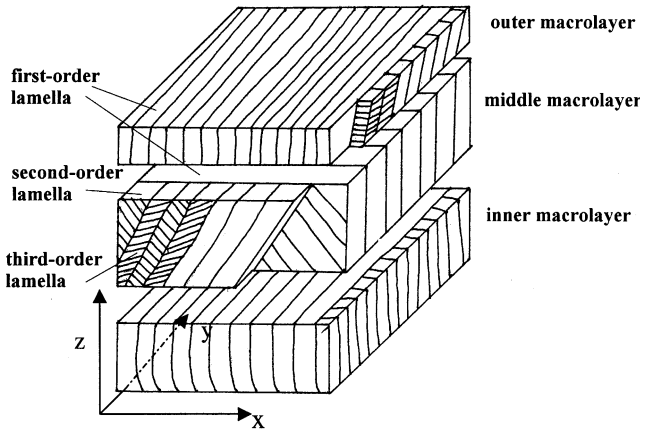

Fig. 1. A simplified schematic drawing of the crossed-lamellar structure of *S. gigas*. Each macroscopic layer is composed of first-, second- and third-order lamellae.

2. *Strombus gigas* (conch shell)

S. gigas is part of the *Conus* family of shells; this shell, also known as conch, has a logarithmic spiral shape. *Conus* shells have a cross-lamellar structure consisting of lath-like aragonite crystals (99.9% of shell weight) and a tenuous organic layer (0.1 wt.%). This 'plywood' structure is depicted schematically in Fig. 1. The conch microstructure is composed of three macrolayers (outer, middle, and inner). The macrolayers are composed of first-order lamellae with each first-order lamella subdivided into second-order lamellae, which are further subdivided into third-order lamellae. This tessellated structure is very effective in deflecting cracks and delocalizing damage. These three macrolayers are arranged into first-order lamellae forming a 0/90/0° pattern. The second-order lamellae composing the middle macrolayer are oriented ± 35–45° to the first-order lamellae. These second-order lamellae in turn consist of single-crystal third-order lamellae. Fine growth twins at an atomic scale are part of each third-order lamella [9]. The organic matrix with its 0.1 wt.% has only been observed by TEM as an electron dense layer that envelops each of the third order lamellae [10].

Laraia and Heuer [11] performed four-point bending tests on *S. gigas* shells with the shell interior and exterior surfaces as the loading surfaces. They found flexural strengths of about 100 MPa, slightly over one half the strength of abalone. With the exterior surface loaded in tension, the failure occurred catastrophically.

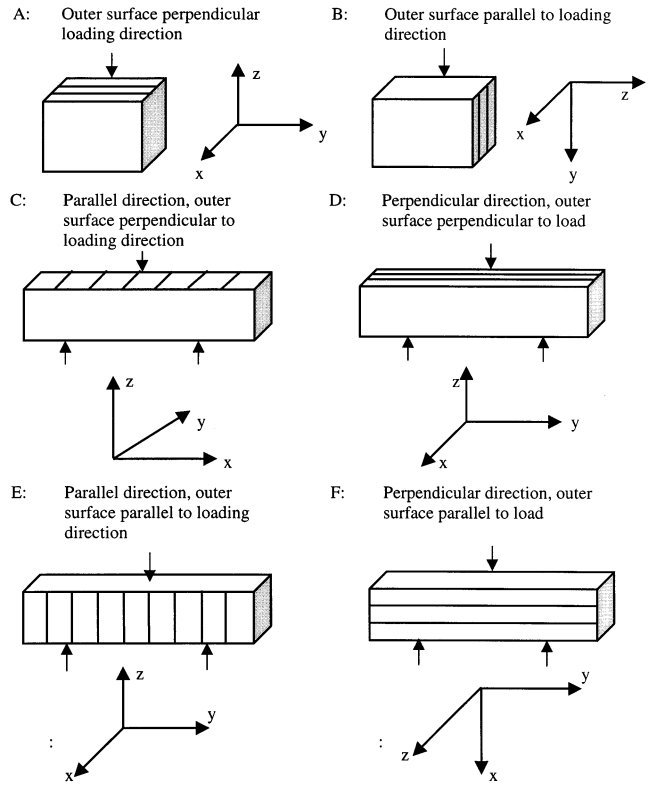

Fig. 2. Conch compression and three-point bending configurations. The hatched areas represent the outer surface orientation.

However, when loaded with the interior surface in tension, catastrophic failure did not always occur. This highlights the anisotropic properties of shells with crossed-lamellar microstructures, which leads to a 'graceful failure' in some orientations. Another indication of the anisotropic mechanical behavior of crossed-lamellar shells can be found in Currey and Kohn [12]. They found flexural strengths (in three-point bending) of shells of *Conus striatus* in the range of 70–200 MPa depending on the orientation. Laraia and Heuer [11] identified several toughening mechanisms: crack branching (i.e. the microstructure forces the cracks to follow a tortuous path), fiber pullout, microcracking (microcracks follow interlamellar boundaries), crack bridging, and microstructurally induced crack arrest. Jackson et al. [13] and Currey [14] also studied the mechanical properties of nacre (or mother-of-pearl, a highly filled ceramic composite of mollusk shells).

3. Experimental approach

The shells studied herein were purchased at a local shell shop (La Jolla, CA) in dry condition. All samples were cut out of the same shell to minimize varying test results due to differences in shell history or age. The first cuts were made by hand, using a hacksaw with an abrasive blade. After obtaining pieces of appropriate size, a high-speed diamond saw was used for further sectioning. Long flat areas with a minimum length of 40 mm and cross sectional areas of about 5×5 mm were kept for producing three-point bend samples. The compression test samples were cut to cubes with approximately 5 mm sides. Care was taken to obtain parallel sides and 90° angles and also to mark the side of the exterior layer. The three-point bend samples of the conch shell were machined with two different orientations, parallel and perpendicular to the shell axis, which also corresponds to parallel and perpendicular to the structure of the outer macrolayer. Fig. 2 gives an overview of the different test configurations. The hatched lines drawn on each conch sketch represent the layered structure of the outer macrolayer; the coordinate systems correspond to that in Fig. 1. The lines drawn on surface are parallel to the conch spiral axis; the hatched surface represents the outer surface (direction *yy* in Fig. 1).

For the compression tests, the conch was tested parallel and perpendicular to the outer surface. Four different conch bend configurations were tested: two with the outer layer perpendicular to the load (with the interior layer in tension) and two with the outer layer parallel to the loading direction. The quasi-static three-point bend tests were conducted under displacement control with a crosshead speed of 0.1 mm min^{-1}.

The samples for the dynamic compression and three-point bend tests were sectioned in the same manner as the samples for quasi-static testing. A momentum-trapped split Hopkinson (Kolky [15]) bar was used for the dynamic tests; details of the momentum trapping device are given elsewhere [16]. All dynamic compression tests were carried out at rates between 10×10^3 and 25×10^3 GPa s^{-1}.

4. Results and discussion

4.1. Mechanical properties

There are many uncertainties in performing mechanical tests with mollusk shells. Besides the varying layer thickness, there are a considerable number other natural shell irregularities such as flaws, existing microcracks or even macrocracks, and perforations made by foreign organisms. Additionally, there is some uncertainty about a given shell's history, including its age and degree of hydration. As such, the determination of the mechanical properties of these shells requires a statistical analysis in order to be quantitatively evaluated. A Weibull analysis [17] was applied to the quasi-static and dynamic compression tests by means of the following equation:

$$P(V) = \exp\left[-\left(\frac{\sigma}{\sigma_0}\right)^m \right] \quad (2)$$

where $P(V)$ is the survival probability, σ_0 and m are Weibull parameters obtained experimentally, and σ is the strength. The Weibull distribution is usually used for flexural strengths. Nonetheless, it is herein applied for compression testing, as this test configuration provided the largest amount of data. For a detailed treatment of the Weibull analysis under a variety of loading configurations, see Wachtman [18].

Fig. 3(a) shows representative stress–strain curves of conch samples with loading perpendicular to the outer surface (configuration A; Fig. 2). The compressive strengths are between 180 and 210 MPa, and failure initiates at strains of 0.007–0.008. The material undergoes a damage-induced softening after the maximum of the stress–strain curve is reached. The softening slope (about 8 GPa) is about one-quarter of the elastic stiffness, E, which is approximately 30 GPa. In contrast, monolithic ceramics usually fracture catastrophically. Four quasi-static stress strain curves of the conch shell loaded parallel to the outer surface are shown in Fig. 3(b) (configuration B; Fig. 2). Failure occurs at strains between 0.009 and 0.013, and at stress levels between 210 and 310 MPa. Three dynamic stress–strain curves of conch samples compressed perpendicular to the outer surface are shown in Fig. 3(c). The failure strains are between 0.005 and 0.012, and the maximum stress is found to be between 230 and 300 MPa. Fig. 3(d) displays the dynamic stress–strain response of the conch when loading parallel to the outer surface. The maximum stress is between 320 MPa and 410 MPa, and failure strains between 0.008 and 0.011. Due to the variation of the strength from specimen to specimen, it is difficult to draw conclusions by comparing individual test results.

Fig. 4(a) and (b) show the Weibull functions and the fracture probabilities of the quasi-static and dynamic compression tests of the conch, respectively. The results of tests with the outer surface both parallel and perpendicular to the loading direction are given. The Weibull parameter 'm' for the parallel direction is 5.07 and for

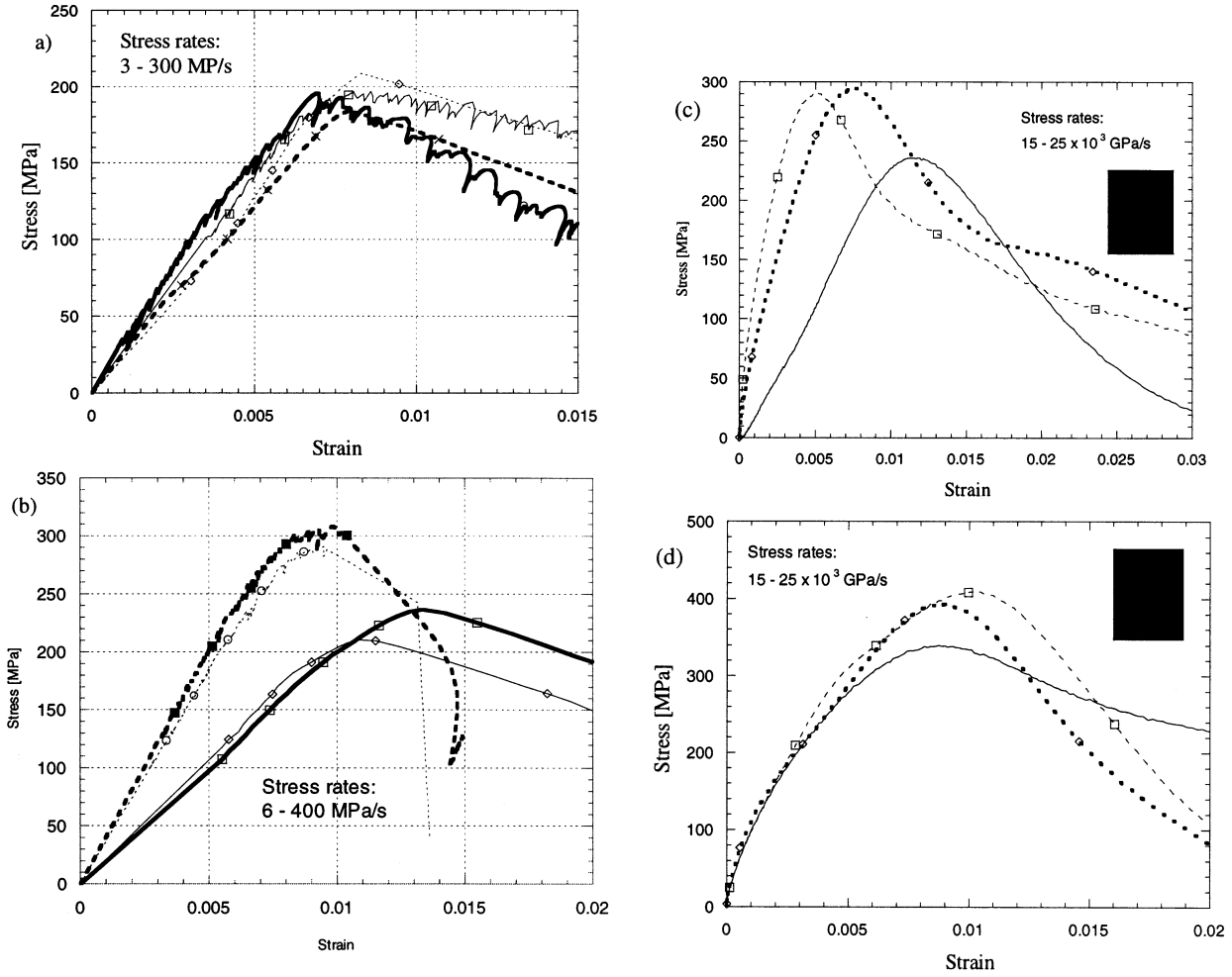

Fig. 3. Compressive stress–strain curves of conch samples: (a) quasi-static, loading perpendicular to outer surface (configuration A, Fig. 2); (b) quasi-static, loading parallel to outer surface (configuration B, Fig. 2); (c) dynamic, loading perpendicular to outer surface(configuration A, Fig. 2); (d) dynamic, loading parallel to outer surface (configuration B, Fig. 2).

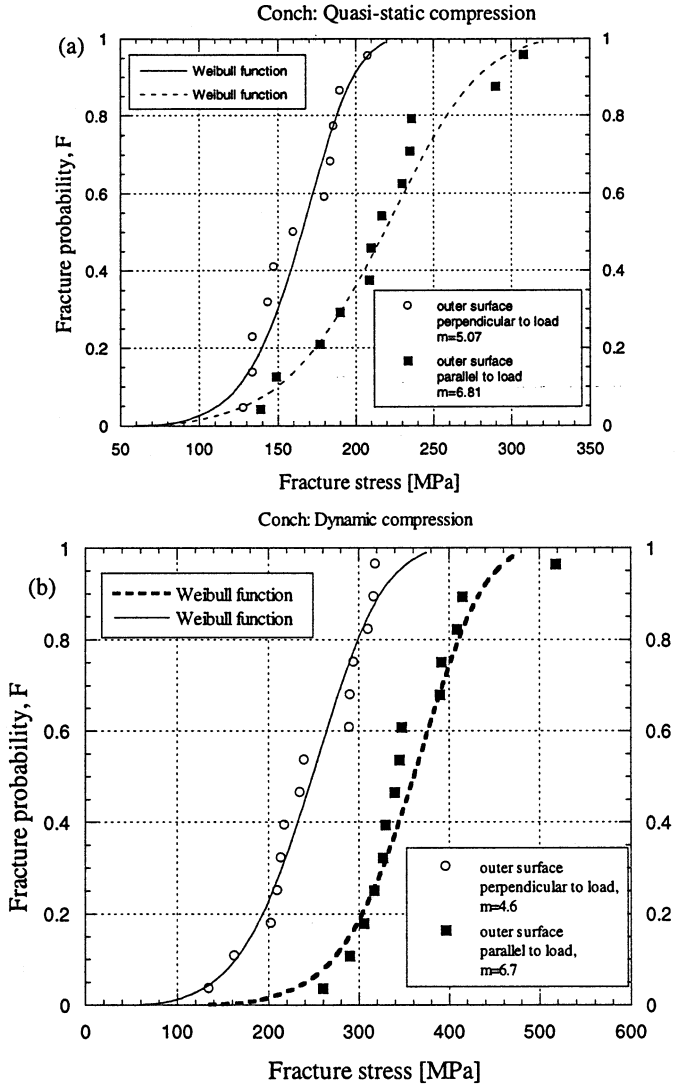

Fig. 4. Weibull distribution of the conch; (a) quasi-static and (b) dynamic compression testing.

Table 1
Maximum stresses (in MPa) of four different testing orientations in three-point bending outer layer perpendicular to loading outer layer parallel to loading

Orientation C	Orientation D	Orientation E	Orientation F
72	24	84	38
55	23	74	20
49		64	
52(avg.)	24(avg.)	74(avg.)	29(avg.)

the perpendicular loading direction is 6.81 (quasi-static). It can be seen that the 50% fracture probabilities ($P(V) = 0.5$) of the quasi-statically tested samples are equal to 166 and 218 MPa for the perpendicular (configuration A) and the parallel test direction (configuration B), respectively. In dynamic testing, the 50% fracture probabilities are equal to 249 MPa (outer surface perpendicular to load; configuration A in Fig. 2) and 361 MPa (outer surface parallel to load; configuration B in Fig. 2). Thus (a), the conch is stronger in compression with the loading direction parallel to the outer surface, and (b) the dynamic strength is significantly higher ($\sim 50\%$) than the quasi-static strength. The quasi-static and dynamic results are remarkably consistent, and the Weibull slopes '*m*' show a good correspondence.

The results of the bending tests are shown in Table 1. Four orientations were tested, as marked in Fig. 2. Orientations C and E showed the highest strength, while orientations D and F had a strength approximately 50% of orientations C and E. The strong orientation represents the direction parallel to the conch 'opening' (axis of spiral). These results are consistent with the compressive strengths, which are also higher in the 'parallel' orientation (B in Fig. 2).

4.2. Characterization of damage in Strombus gigas

In compression loading, brittle materials tend to fail by an axial splitting mechanism, in which the fracture is parallel to the loading direction (e.g. [19]). This axial splitting mechanism leads to the formation of separate columns of material from one single specimen, which will lead to buckling of the individual columns and their successive fracture. The axial splitting process is initiated at existing flaws, by tensile stresses generated perpendicular to the loading direction. This axial splitting mechanism is inhibited when there is lateral confinement. In the conch shells, cracks also tended to propagate along the loading direction when tested in compression. Damage in a compression sample after testing with the outer surface perpendicular to loading direction is presented in Fig. 5. It can be seen that a macrocrack, after passing through the outer macrolayer (see arrow A), is bifurcated and deflected by the middle macrolayer. The deflection angle is approximately 45° (arrows B). A closer look at the outer layer reveals multiple channel cracking along first-order interfaces and extensive microcracking through interfaces between second-order lamellae (Fig. 5(b)). The layers undergo a systematic deflection which is known as a kinking (or microplastic buckling) phenomenon; this is described in greater detail in a separate paper [20]. The optical micrograph in Fig. 6(a) shows that macrocracks change their direction again when reaching the inner macrolayer, which is composed of first-order lamellae having the same orientation as the ones in the outer macrolayer. Within the middle macrolayer, microcracks follow a tortuous path, deflected at the organic-ceramic interfaces before cracking through the second-order lamellae. The resulting crack has a zigzag pattern shown in detail in Fig. 6(b). This is clearly a mode of failure in which one single crack is delocalized, con-

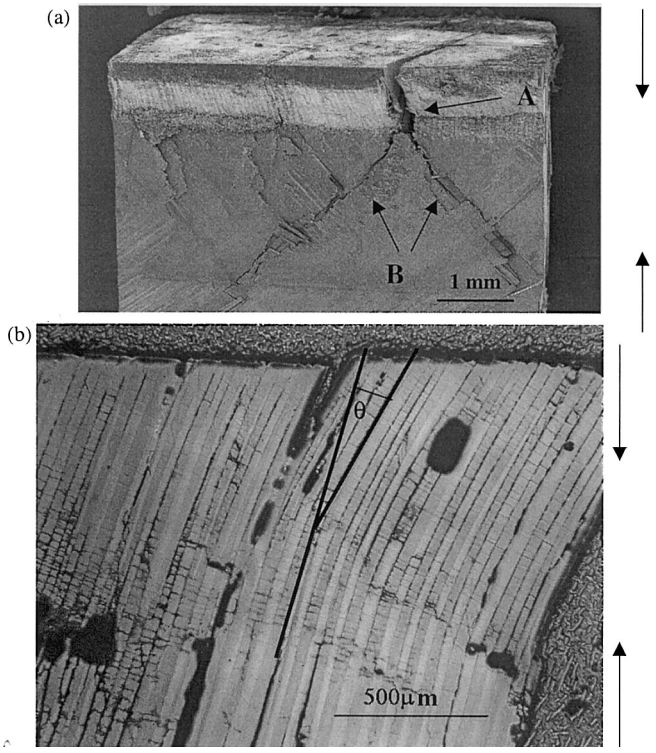

Fig. 5. (a) SEM taken after quasi-static compression testing with outer surface perpendicular to loading direction (loading indicated); (b) sliding along second-order lamellae in outer layer, creating a rotation θ and kinking.

tributing to toughening. The fracture pattern is readily understood, by examination of Fig. 1: a crack in plane '*yz*' coming through the outer macrolayer is deflected and has to bifurcate, as it penetrates into the middle macrolayer (note the 45° bifurcation seen in Fig. 5(a)). When the crack reaches the inner macrolayer (bottom region in Fig. 1) it can again orient itself into an 'axial splitting' configuration (seen in Fig. 6(a) bottom part).

The compression tests on the conch shell with the outer surface parallel to the loading direction revealed maximum stresses approximately 60 MPa higher than in the perpendicular direction. The difference is attributed to the highly anisotropic crossed-lamellar structure. Turning the sample into the 'strong' direction causes the middle layer, with its enhanced strength, to be directly in contact with the two loading platens of the test apparatus. Cracks now have to pass through the middle layer by cracking through single first-order lamella (arrows C in Fig. 7(a)) by running through second and third-order lamellae. In the 'weak' direction, cracks can circumvent the middle layer through first-order interfaces. The delocalization of damage is evident in Fig. 7(b) in which the lateral surface of a damaged specimen is shown. The interfaces, where relative motion or separation occurred, become visible optically, whereas they are invisible in the undeformed regions; therefore, the complex pattern of interfacial sliding becomes visible. Interfaces between second and third-order lamellae are visible and are marked by arrows A and B, respectively. It is speculated that these displacements are self-accommodating (i.e. that they occur in an compatible manner, shown in Fig. 8, where the layers are depicted prior to and after deformation). This self-accommodating process, which occurs by the

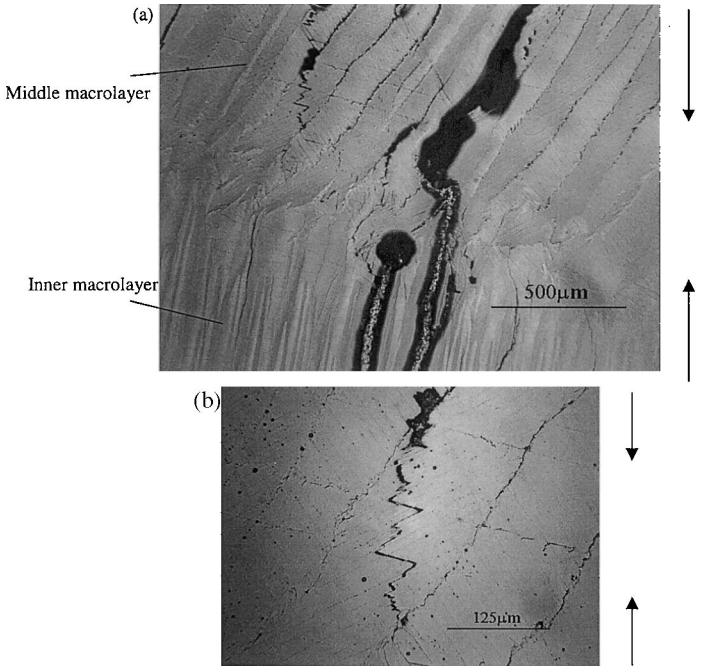

Fig. 6. (a) Cracking pattern at middle layer and middle/inner layer interface; (b) middle layer: cracks at second- and third-order interfaces. Loading direction marked on r.h.s.

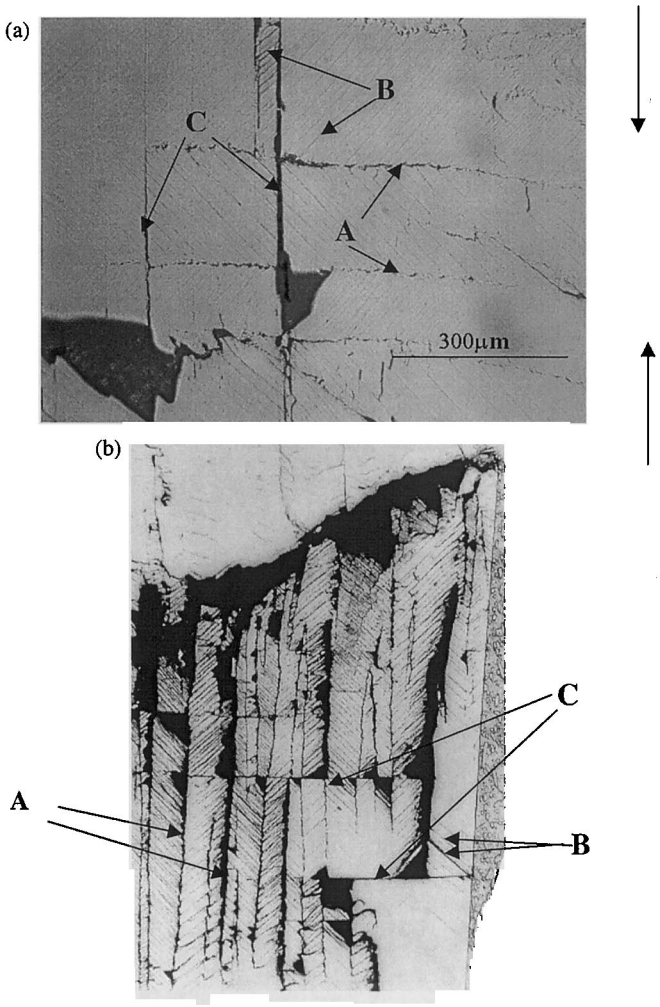

Fig. 7. (a) Middle layer: cracking along interfaces of second (arrow A) and third-order (arrow B) lamellae, as well as trans-lamellar cracking (arrow C); (b) lateral surface of compressive specimen after partial failure.

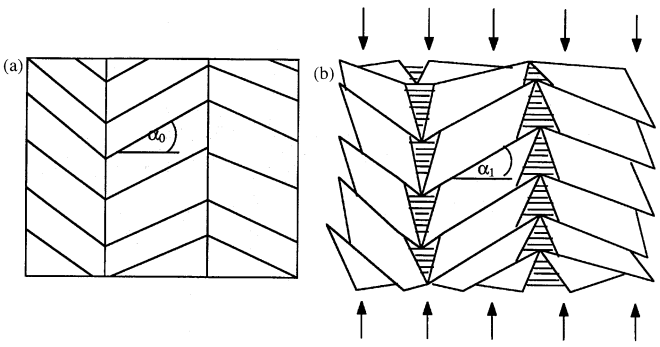

Fig. 8. Self-accommodating movement of blocks of third-order lamellae by interfacial sliding; gaps created at interfaces by rotations ($\alpha_0 > \alpha_1$); (a) initial configuration; (b) deformed configuration.

viscoplastic deformation of the organic layers, produces single incompatible edges (hatched gaps in Fig. 8) at the interface due to the rotation that accompanies the deformation. However, the self-accommodation process is not complete. There is a third family of cracks in Fig. 7(b) (marked by arrows C), which traverse the lamellae and are very straight and parallel. Their parallelism, as well as regular pattern, is an indication of an organized growth mechanism, and a possible growth sequence is shown in Fig. 9. The back first-order lamella contains three interfaces (Fig. 9(a)), which initially fail forming a crack of length of 2a (Fig. 9(b)). This crack size exceeds the critical flaw size for the material at the imposed load and therefore grew through the material, penetrating in the adjacent layers. After the cracks traverse the front first-order lamella, which is shown in Fig. 9(c), they would form a pattern similar to the one shown in Fig. 7(b) marked by arrows C.

The fracture surfaces observed by scanning electron microscopy (SEM) are shown in Fig. 10. Fig. 10(a) shows the successive parallel third-order lamellae; the irregular step-like nature of the fracture is clear. Steps are necessary to transition across the fracture plane from one lamella to the next. The higher magnification view of Fig. 10(b) shows (lower right side) one lamella; the fracture at the interface creates a smooth plane (A). The lamella behind (marked by B) is fractured, and the surface resembles broken wood: (fragments of fibers are clearly seen, arrow C). This shows that each third-order lamella is composed of 'wood-like' fibers. These fibers can be seen in Fig. 10 (c), which shows a view of their extremities (the surface is marked A), at the end of the lamella. The diameter of these fibers is not known exactly, but appears to be on the order of 0.5 μm. Thus, a third-order lamella can be envisaged as a wood plank, cut with a rectangular cross-section; the lamella fibers correspond to the wood fibers. Clearly, the complex architecture of the conch shell plays a key role in retarding failure by delocalization of cracks.

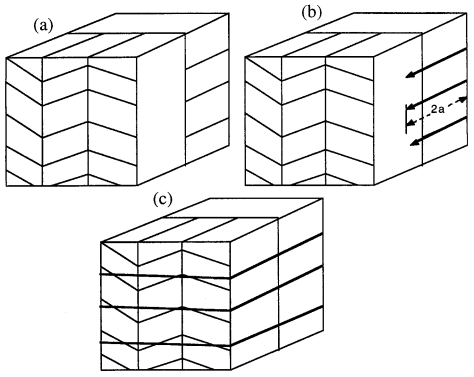

Fig. 9. Sequence of events leading to formation of parallel trans-lamellar cracks: (a) initial configuration; (b) separation of lamellae in back layer initiating crack through frontal layers; (c) complete crack propagation through frontal layers.

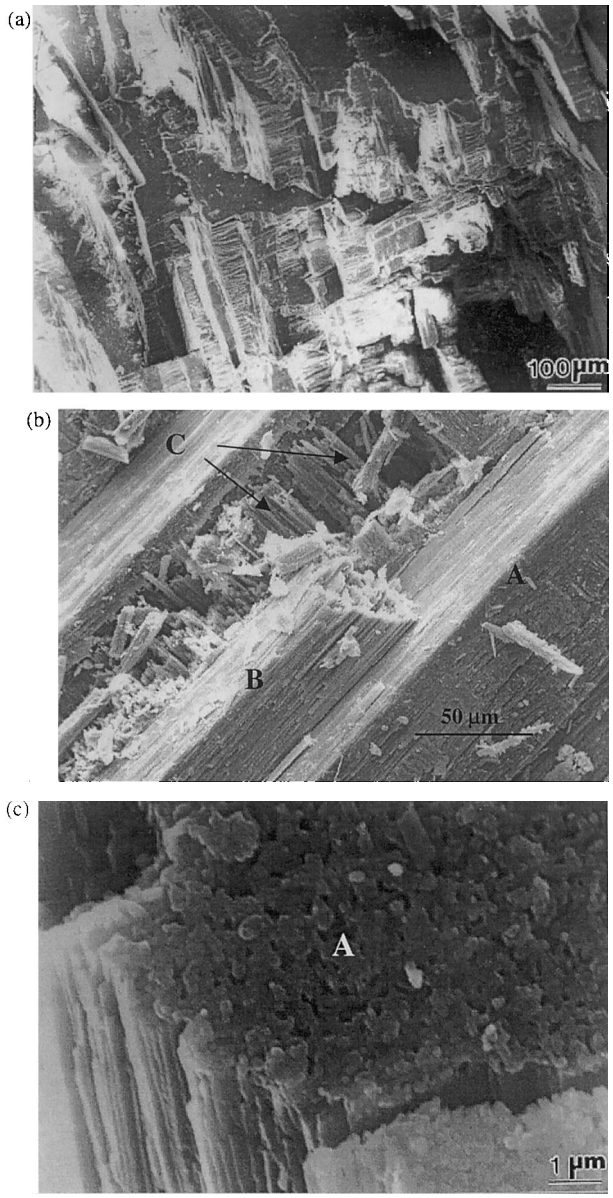

Fig. 10. Fracture surface of conch compression specimens; outer surface parallel to loading direction (configuration B); (a) overall view; (b) broken third-order lamellae; (c) high magnification view of extremity of third-order lamella.

4.3. Damage mechanisms

From the above observations and analysis, it is apparent that the shell structure imparts a significant increase in the toughness of an otherwise brittle monolithic material ($CaCO_3$). Two primary toughening mechanisms were identified: (a) sliding of $CaCO_3$ blocks by means of viscoplastic deformation of the organic interfacial layers (Fig. 11(a)); arrest and deflection of cracks by the viscoplastic layers (Fig. 11(b)). These two basic mechanisms and the fine microstructure, consisting of $CaCO_3$ platelets, lead to delocalization of failure, by which one single sharp crack is replaced by a large number of smaller cracks, within a broader region (Fig. 11(c)). It is of interest, and will serve as the basis of further study, to determine in a quantitative manner the amount of energy that can be dissipated by each of these toughening mechanisms.

5. Summary and conclusions

Mechanical tests were carried out assess the mechanisms of damage accumulation in the conch shells. The strength of these shells shows a considerable variation, and is well represented by a Weibull distribution with parameter m varying between 2.5 and 6.8. The compressive strengths of the conch ($P(V) = 0.5$) are 166 and 218 MPa for testing perpendicular (configuration A) and parallel (configuration B) to the surface, respectively. The dynamic compressive strength is approximately 50% higher than the quasi-static value. The ratio between the strength perpendicular to the outer surface and parallel to the outer surface, given in terms of $P(V) = 0.5$, is equal to 0.7 for both quasi-static and dynamic testing. The tensile strength, as measured from flexure tests, varies from 24 to 74 MPa, depending on orientation (Table 1); the average is 46.5 MPa. The ratio between compressive and tensile (as measured by bending test) strengths is 4.1. This is a surprisingly low ratio between compressive and tensile strength, considerably below that of monolithic ceramics, typically in the 8–12 range. This surprising response is due to the toughening mechanisms operating. The higher dynamic strength for conch, compared to its quasi-static

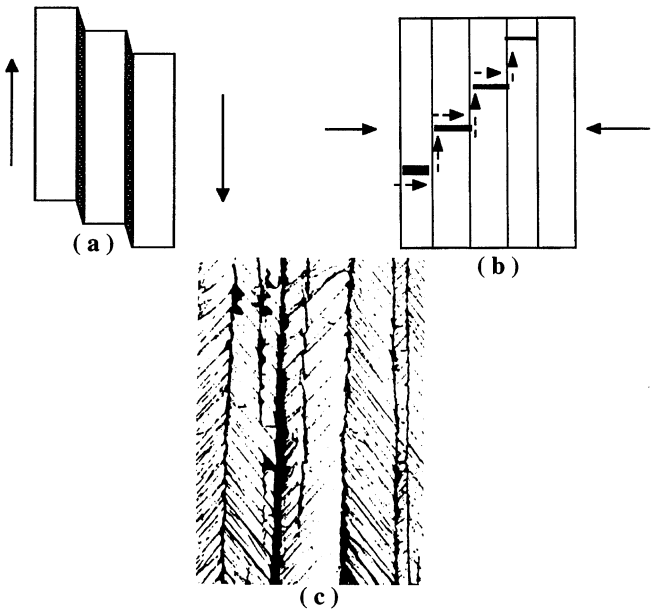

Fig. 11. Principal mechanisms of damage accumulation in shells: (a) viscoplastic deformation of organic layers; (b) crack deflection by organic layers; (c) delocalization of damage.

strength, can be attributed to the strain-rate sensitivity of the organic layer. The ceramic phase ($CaCO_3$) is not expected to show such a strain–rate dependence, since ceramics require strain rates on the order of 10^3 s^{-1} to exhibit significantly noticeable effects, and the strain rates of the experiments carried out herein are on the order of 50–100 s^{-1}. Gray et al.[21] carried out dynamic experiments on Adiprene L-100:a rubber. They found a very high strain-rate sensitivity; the yield stress increased from 2 to 6 MPa, with an attendant eight-fold increase in the apparent loading modulus. In the current experiments, the strain rate experienced by the organic layers is much higher than the global strain rate, because deformation is concentrated in them.

It can be concluded that the hierarchical structure of the conch shells enhances their toughness in a significant fashion, by providing several important mechanisms for controlling damage: (a) viscoplastic deformation of organic layers; (b) crack deflection by organic layers; and (c) delocalization of damage.

Acknowledgements

This research was partially supported by the US Army Research Office under the MURI program (Contract no. DAAHO4-96-10376). Mr. Menig worked at UCSD as part of an exchange program between the University of Karlsruhe (TH) and the University of California, San Diego. Appreciation is extended to Professor Otmar Vöhringer for making this exchange possible and the Humbolett Foundation for a Senior Scientist Award for MAM. We would like to thank David Harach and Dr Y.-J. Chen for setting up the quasi-static test configurations and Dr A. Strutt for his assistance in the SEM analysis. Professor G. Ravichandran, California Institute of Technology, kindly allowed us to use his laboratory to perform some of the quasi-static compression and flexural tests; his help and that of his student, S. Zhuang, is gratefully acknowledged. We would like to thank Dr G. Mayer (US ARO) for having stimulated our interest in this topic and Professor Sarikaya (University of Washington) for insightful discussions.

References

[1] M.F. Ashby, Materials Selection in Mechanical Design, Butterworths-Heinemann, London, UK, 1999.
[2] E. Baer, Adv. Polym. Sci. Am. 255 (4) (1986) 156.
[3] E. Baer, A. Hiltner, R.J. Morgan, Phys. Today (1992) 60–67.
[4] J.F.V. Vincent, Structural Biomaterials, Princeton University Press, Princeton, NJ, 1991.
[5] A.V. Srinivasan, G.K. Haritos, F.L. Hedberg, Appl. Mech. Rev. 44 (1991) 463–482.
[6] M. Sarikaya, Microsc. Res. Tech. 27 (1994) 360–375.
[7] M. Sarikaya, I.A. Aksay, Nacre of abalone shell: a natural multi-functional nanolaminated ceramic-polymer composite material, in: S. Case (Ed.), Results and Problems in Cell Differentiation in Biopolymers, Springer Verlag, Amsterdam, 1992, pp. 1–25.
[8] M. Sarikaya, K.E. Gunnison, M. Yasrebi, J.A. Aksay, Mechanical Property — Microstructural Relationships in Abalone Shell, vol. 174, Materials Research Society, Pittsburgh, PA, 1990, pp. 109–116.
[9] L.F. Kuhn-Spearing, H. Kessler, E. Chateau, R. Ballarin, A.H. Heuer, J. Mater. Sci. 31 (1996) 6583–6594.
[10] S. Weiner, Am. Zool. 24 (4) (1984) 945–952.
[11] J.V. Laraia, A.H. Heuer, J. Am. Ceram. Soc. 72 (1) (1989) 2177–2179.
[12] J.D. Currey, A.J. Kohn, J. Mater. Sci. 11 (1976) 1614–1623.
[13] A.P. Jackson, J.F.V. Vincent, R.M. Turner, Proc. R. Soc. London B234 (1988) 415–440.
[14] J.D. Currey, Proc. R. Soc. London B196 (1977) 443.
[15] H. Kolsky, Proc. R. Soc. B62 (1949) 676.
[16] S. Nemat-Nasser, J.B. Isaacs, J.E. Starrett, Proc. R. Soc. A435 (1991) 371.
[17] W. Weibull, Ingenioersvetenskapsakad. Handl. 151 (1939) 1–45.
[18] J.B. Wachtman, Mechanical Properties of Ceramics, Wiley-Interscience, New York, NY, 1996.
[19] M.A. Meyers, Mechanical Behavior of Materials, Prentice Hall, Upper Saddle River, NJ, 1999, pp. 418–421.
[20] R. Menig, M.H. Meyers, M.A. Meyers, K.S. Vecchio, Acta Mater. 48 (2000) 2383–2398.
[21] G.T. Gray, III, W.R. Blumenthal, C.P. Trujillo, R.W. Carpenter, II, J. Phys. IV Fr. 7 (1997) C3–523.